X-ray damage to the Mn_4Ca complex in single crystals of photosystem II: A case study for metalloprotein crystallography

Junko Yano*[†‡], Jan Kern[‡§], Klaus-Dieter Irrgang[§], Matthew J. Latimer[¶], Uwe Bergmann[¶], Pieter Glatzel[‖], Yulia Pushkar*[†], Jacek Biesiadka**, Bernhard Loll**, Kenneth Sauer*[†], Johannes Messinger[†††‡‡], Athina Zouni[§‡‡], and Vittal K. Yachandra*[‡‡]

*Melvin Calvin Laboratory, Physical Biosciences Division, Lawrence Berkeley National Laboratory, Berkeley, CA 94720; [†]Department of Chemistry, University of California, Berkeley, CA 94720; [§]Max-Volmer-Laboratorium für Biophysikalische Chemie, Technische Universität, Strasse des 17 Juni 135, D-10623 Berlin, Germany; [¶]Stanford Synchrotron Radiation Laboratory, 2575 Sand Hill Road, Menlo Park, CA 94305; [‖]European Synchrotron Radiation Facility, 6 Rue Jules Horowitz, BP 220, F-38043 Grenoble Cedex, France; **Institut für Kristallographie, Freie Universität, Takustrasse 6, D-14195 Berlin, Germany; and [††]Max-Planck-Institut für Bioanorganische Chemie, Stiftstrasse 34-36, D-45470 Mülheim an der Ruhr, Germany

Communicated by Judith P. Klinman, University of California, Berkeley, CA, June 28, 2005 (received for review April 24, 2005)

X-ray absorption spectroscopy was used to measure the damage caused by exposure to x-rays to the Mn_4Ca active site in single crystals of photosystem II as a function of dose and energy of x-rays, temperature, and time. These studies reveal that the conditions used for structure determination by x-ray crystallography cause serious damage specifically to the metal-site structure. The x-ray absorption spectra show that the structure changes from one that is characteristic of a high-valent $Mn_4(III_2,IV_2)$ oxo-bridged Mn_4Ca cluster to that of Mn(II) in aqueous solution. This damage to the metal site occurs at a dose that is more than one order of magnitude lower than the dose that results in loss of diffractivity and is commonly considered safe for protein crystallography. These results establish quantitative x-ray dose parameters that are applicable to redox-active metalloproteins. This case study shows that a careful evaluation of the structural intactness of the active site(s) by spectroscopic techniques can validate structures derived from crystallography and that it can be a valuable complementary method before structure–function correlations of metalloproteins can be made on the basis of high-resolution x-ray crystal structures.

manganese | oxygen evolution | water oxidation | x-ray spectroscopy

Oxygen, which supports all aerobic life, is abundant in the atmosphere because of its constant regeneration by photosynthetic water oxidation by green plants and cyanobacteria. The structure of the catalytic Mn_4Ca complex that generates oxygen by the oxidation of water has been the subject of intense study ever since Mn was identified as an essential element (1–4). The structural features of the Mn complex have been studied extensively with x-ray absorption (5–7), EPR (8–11), and FTIR spectroscopies (12, 13). In addition, the four recent x-ray crystallography studies of photosystem II (PS II) (14–17) promise to add valuable information to our knowledge about the structure of PS II and the Mn_4Ca complex. However, at present, there are serious discrepancies among the models of the structure of the Mn_4Ca complex in the published x-ray crystallography studies, and there are inconsistencies with x-ray, EPR, and FTIR spectroscopic data (5, 13, 18–23). This disagreement is, in all likelihood, predominantly a function of x-ray-induced damage to the catalytic metal site and differences in the interpretation of the electron density at the presently available resolution (3.2–3.8 Å). Therefore, the reported model of the Mn_4Ca complex at atomic detail (16) cannot be based on the diffraction data only and is highly unlikely.

The most common criterion used to measure x-ray damage during crystallography has been the loss of intensity and resolution of the diffraction spots, referred to as the diffraction power of the crystal (24). An x-ray dose of 2×10^7 grays at 77 K was determined by Henderson (25) to result in a 50% reduction in diffraction power and is often used as a benchmark for protein crystallography studies. However, it has been recognized that specific damage to the crystal can occur at lower doses, especially at water-accessible active sites and at redox-active metal sites (24, 26–29). Nevertheless, there are no systematic studies of damage to metal sites, and the discussions have been qualitative (30, 31).

It is therefore imperative to monitor the x-ray-induced effects on the electronic and geometric structure of the Mn_4Ca complex *in situ* to monitor the x-ray-induced damage or lack thereof of the Mn_4Ca complex to validate the structures based on x-ray crystallography and to develop protocols that mitigate the damage in future crystallography studies. In this case study, we used x-ray absorption spectroscopy (XAS) at the Mn K edge to conduct a systematic study of the x-ray damage to the oxygen-evolving Mn_4Ca site of PS II single crystals. XANES (x-ray absorption near edge spectroscopy) provides information about the electronic structure of the metal site and is sensitive to even small changes in charge or oxidation states of the metal. EXAFS (extended x-ray absorption fine structure) is sensitive to metal–metal/ligand distances to an accuracy of 0.02 Å and with 0.14-Å resolution (32) for the data presented here. We measured the damage to the catalytic metal site as a function of time, temperature, dose,[§§] and energy of x-rays by monitoring the Mn K edge XANES and EXAFS. The results show that the damage to the active metal site follows a very different x-ray dose profile compared with the loss of diffractive power of the crystals as established by x-ray crystallography (25).

The Mn XANES data from PS II single crystals show that under the conditions of the recently published x-ray diffraction measurements, the Mn is largely reduced to Mn(II) from $Mn_4(III_2,IV_2)$ present in the native S_1 state cluster. Moreover, the EXAFS spectrum changes significantly from one that is characteristic of a high-valent multinuclear oxo-bridged Mn_4Ca cluster to one that is typical of mononuclear hexacoordinated Mn(II) in solution.

Freely available online through the PNAS open access option.

Abbreviations: EXAFS, extended x-ray absorption fine structure; PS II, photosystem II; XANES, x-ray absorption near edge spectroscopy; XAS, x-ray absorption spectroscopy; FT, Fourier transform.

[‡]J.Y. and J.K. contributed equally to this work.

[‡‡]To whom correspondence may be addressed. E-mail: messinger@mpi-muelheim.mpg.de, zouni@phosis1.chem.tu-berlin.de, or vkyachandra@lbl.gov.

[§§]The common unit for dose used in x-ray spectroscopy is photon density or photons per unit area at a given energy. The unit used in crystallography is the gray (J/kg). We show both of these units in Fig. 2, for purposes of comparison. A common dose limit for crystallography studies is 2×10^7 grays (25), which, at 6.6 keV, corresponds to 1×10^{10} photons per μm^2; at 13.3 keV, it is 4.4×10^{10} photons per μm^2.

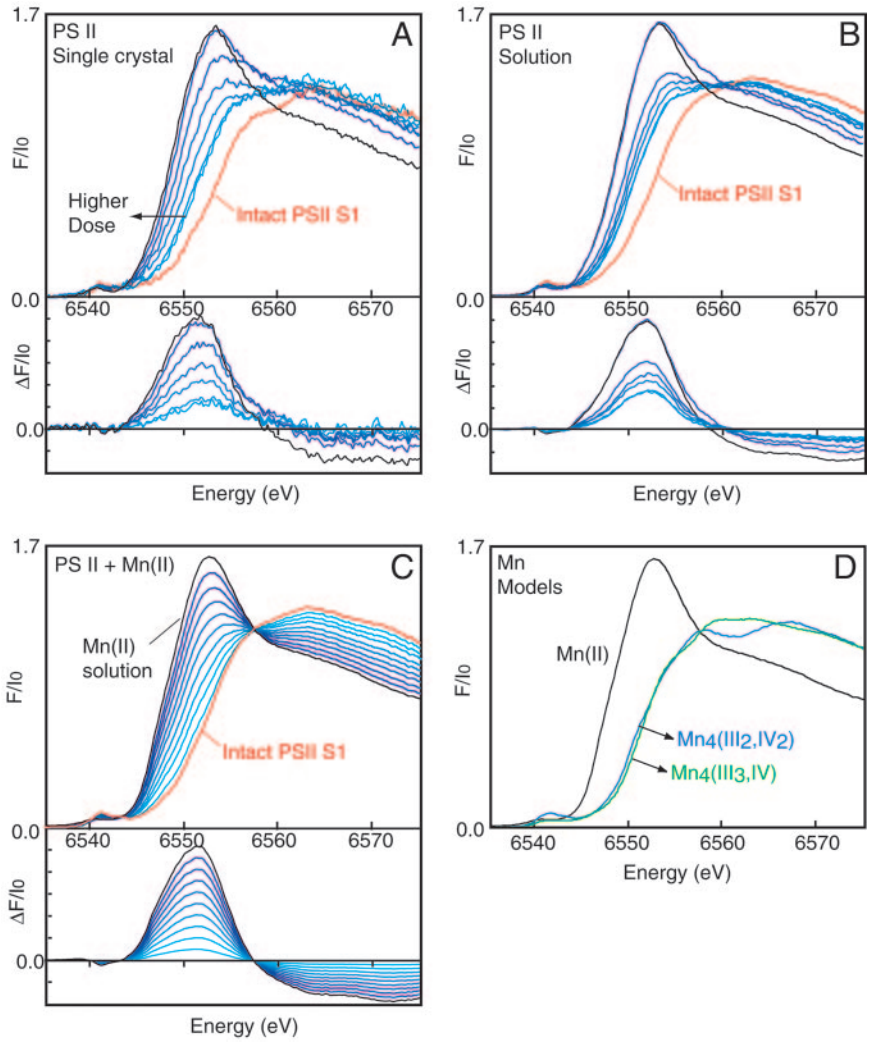

Fig. 1. Mn XANES of PS II versus x-ray dose and XANES of inorganic model compounds. (*A*) Mn K edge shift of PS II crystals as a function of x-ray dose at 13.3 keV (0.933 Å) and 100 K (*Upper*) and the difference spectra (*Lower*). The spectrum at the highest inflection point energy is from an undamaged PS II crystal. The x-ray doses used for exposure are 0.14, 0.21, 0.25, 0.54, 0.95, 2.3, and 5.0×10^{10} photons per μm^2 (light-blue to black lines). An average dose of $\approx 3.5 \times 10^{10}$ photons per μm^2 was used for x-ray diffraction studies. The exposure was at 100 K, and all XANES was collected at 10 K at low dose (1×10^7 per μm^2). XANES and difference spectra show that the increase in amplitude at ≈6,552 eV provides definite evidence for the photoreduction to Mn(II) in PS II crystals by exposure to x-rays (see *C*). At a dose of 2.3×10^{10} photons per μm^2, equal to 66% of the average dose used for diffraction measurements, 80% of the Mn in PS II is present as Mn(II). (*B*) A similar trend in the XANES (*Upper*) and the difference spectra (*Lower*) is seen for PS II solutions. The x-ray doses used for exposure were 0.03, 0.05, 0.10, 0.17, 0.32, 0.76, and 1.4×10^{10} photons per μm^2 (light-blue to black lines). At a dose of 1.4×10^{10} per μm^2, equal to 40% of the average dose used for diffraction measurements, 90% of the Mn in PS II is present as Mn(II). (*C*) The changes in the XANES spectra from an intact PS II sample as a function of addition of 10% increments of the XANES spectrum of aqueous Mn(II) (*Upper*) and the corresponding difference spectra (*Lower*) (light-blue to black lines). The similarity between the difference spectra in *A*, *B*, and *C* is striking, showing the photoreduction of the $Mn(III_2,IV_2)$ in native PS II to Mn(II). (*D*) A comparison of Mn K edge spectra from two tetranuclear complexes, $[Mn_4O_3(OAc)_4(dbm)_3]$ (35, 36) and $[(Mn_2O_2)_2(tphpn)_2](ClO_4)_4$ (37, 38), in oxidation states $Mn_4(III_3,IV)$ and $Mn_4(III_2,IV_2)$ similar to those in intact PS II and from Mn(II) in aqueous solution.

Materials and Methods

PS II crystal samples from *Thermosynechococcus elongatus* were prepared as described by Kern *et al.* (33). The PS II solution samples were prepared at a concentration of ≈5 mM chlorophyll *a* by dissolving crystals in a buffer containing ≈50% glycerol, 50 mM Pipes-NaOH (pH 7.0), 3 mM $CaCl_2$, and 0.015% *n*-dodecyl-β-D-maltoside.

X-Ray Dose for Diffraction Studies. The average total number of x-ray photons per area or dose that each segment of PS II crystal was exposed to during typical x-ray diffraction studies at the three synchrotron radiation sources by three different groups are as follows: (*i*) European Synchrotron Radiation Facility, beamline ID 14-2, ≈ 2.25–4.5×10^{10} photons per μm^2 at 13.3 keV (0.933 Å) (14, 17), (*ii*) SPring-8 (Hyogo, Japan), beamline BL41XU, 1–6×10^{10} photons per μm^2 at 12.4 keV (1 Å) (ref. 15 and N. Kamiya and J.-R. Shen, personal communication), and (*iii*) Swiss Light Source (Villigen, Switzerland), beamline S065A, 1.75–3.5×10^{10} photons per μm^2 at 13.3 keV (0.933 Å) (ref. 16 and S. Iwata, personal communication). The anomalous diffraction studies were carried out at the Mn K edge at 1.894 Å (6.546 keV) (14, 16, 17) and at 2.254 Å (5.500 keV) (16).

Methodology of Data Collection for X-Ray Spectroscopy. The specific difference of the XAS experiments compared with x-ray crystallography is that (*i*) one can specifically probe the intactness/damage to the Mn_4Ca complex by its known spectroscopic signatures and (*ii*) good signal-to-noise data can be obtained by

using a much lower x-ray dose than that typically required for high-resolution diffraction experiments (25). The x-ray dose and beam size sufficient for collecting XANES and EXAFS data are far less stringent than those required for the diffraction experiments. Moreover, all XAS experiments were performed at 10 K, compared with the 100 K that is normally used during crystallography. It is thereby possible to study the effect of x-rays on the Mn_4Ca cluster without inflicting any additional changes to its structure or oxidation state.

The methodology used for the collection of Mn XANES and EXAFS data and analysis is described in detail in refs. 32 and 34. These studies were carried out on beamline 9-3 and 10-2 at Stanford Synchrotron Radiation Laboratory and at the BioCAT 18ID beamline at Advanced Photon Source (Argonne, IL).

Aligning optics were optimized to produce intensity profiles that were plateaus without the presence of hot spots in the beam profile, slits were used to produce beams of precise shape, and filters were used to obtain beams of requisite dose. The sample was accurately positioned and scanned in the x-ray beam by using precision position encoders and a very low dose of photons ($\approx 1 \times 10^5$ photons per μm^2) in order not to cause any damage to the samples. The XAS spectra from single crystals are dichroic. Therefore, all spectra were collected at a specific orientation of the crystal to the x-ray **e** vector. The x-ray flux was measured by using a calibrated N_2-filled ion chamber placed before the sample. The XANES and EXAFS were collected as fluorescence excitation spectra by using a 30-element energy-discriminating Ge solid-state detector (Canberra, Meriden, CT). The diffraction pattern from the crystals was collected *in situ* by using a Mar 345 detector and was used for indexing the crystals before and after exposure to a given number of x-ray photons.

The following protocol was used for measuring the damage to the Mn_4Ca cluster in PS II crystals and solution samples. For each sample, first a XANES spectrum was collected at low dose (1×10^7 photons per μm^2) at 10 K to ascertain the intactness of the samples. The samples were then exposed to x-rays at 13.3 keV (0.933 Å), the wavelength used for native and heavy-atom derivative diffraction measurements, or at 6.6 keV (1.89 Å), the wavelength used for anomalous diffraction measurements. This exposure was performed at 100 K or at 10 K. X-ray dose and the time required for depositing the dose were varied. The sample was then immediately returned to 10 K if it was at 100 K, and the XANES and/or EXAFS (at a low dose of 1×10^7 photons per μm^2) was collected. The XANES spectrum from successive scans was invariant during these measurements. A new sample was used for each exposure at a particular x-ray dose, which ranged from 0.03×10^{10} to 5×10^{10} photons per μm^2. The x-ray dose was chosen to cover the range typically used at third-generation synchrotron sources and, more specifically, to coincide with those used for all PS II diffraction studies (see above). Experimental conditions, such as x-ray flux of the beamline, exposure time per frame, and beam size, are different for each of the three studies described above (see *Supporting Materials and Methods*, which is published as supporting information on the PNAS web site). Despite differences in experimental conditions, the doses for all of the studies are in a comparable range, and the representative dose for high-resolution data is $\approx 3.5 \times 10^{10}$ photons per μm^2 or 1.6×10^7 grays (at 13.3 keV). In this study, the exposure dose is expressed in units of photons per area and in grays or relative to the representative value for current PS II diffraction studies.

Quantitation of Mn(II) with XANES. XANES spectra from a Mn(II) aqueous sample were added to that from an intact PS II sample in different proportions (Fig. 1*C*) and compared with the XANES spectra obtained from single-crystal and solution PS II samples that had been exposed to a specific dose of x-rays (Fig. 1 *A* and *B*). A direct comparison usually was sufficient to obtain the percentage of Mn(II) present in such samples. We also used the difference spectra (Fig. 1 *A*, *B*, and *C Lower*) and the second derivatives (not shown) of the spectra for obtaining values with an accuracy of ±5% Mn(II).

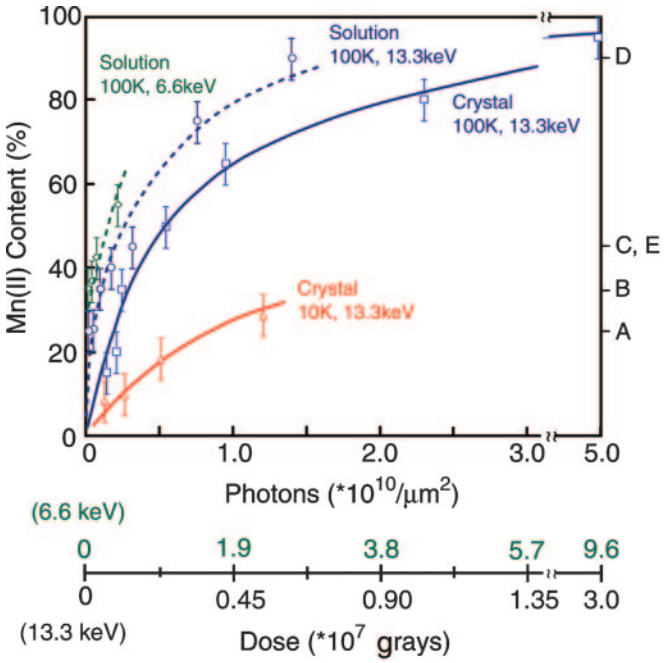

Fig. 2. Increasing Mn(II) content in PS II due to radiation damage. (Solid blue line) Mn(II) content in PS II crystals as a function of x-ray irradiation at 13.3 keV (0.933 Å). The irradiation was carried out at 100 K. The conditions are similar to those during x-ray diffraction data collection. The dose on the abscissa is given in grays and in photons per unit area, units that are commonly used for crystallography and spectroscopy experiments, respectively. The points on the curve represent samples that received between 0.14 and 5.0×10^{10} photons per μm^2. At 66% of the dose (2.3×10^{10} photons per μm^2) compared with the representative average dose (3.5×10^{10} photons per μm^2) used for crystallography, PS II crystals contain ≈80% Mn(II). (Dashed blue line) The damage profile for PS II solution samples is very similar to that seen for crystals, although it is slightly higher for the same dose. EXAFS spectra of samples shown in Fig. 3 are at levels of damage denoted on the right by A, B, C, D, and E. (Dashed green line) The generation of Mn(II) is considerably greater when the x-ray irradiation is at 6.6 keV (1.89 Å), which is the energy at which the anomalous diffraction measurements for PS II were conducted. (Solid blue line) The Mn(II) produced by damage in crystals is considerably decreased when the irradiation is conducted at 10 K, providing a method that could be used to mitigate the effects of radiation damage during crystallography measurements.

Results and Discussion

Fig. 1*A* shows the Mn XANES data collected at 10 K from single crystals subsequent to exposure to a specific dose of 13.3-keV x-rays at 100 K; the typical published x-ray diffraction data of PS II crystals were collected by using 13.3-keV x-rays at 100 K. The Mn XANES spectrum of the intact PS II sample (red line, Fig. 1*A*) has the highest inflection point energy and compares well to the XANES from Mn model compounds in mixed-valent III,IV oxidation states (Fig. 1*D*) (35–38). It is also well established from several other studies that the Mn_4Ca complex in the oxygen-evolving complex of PS II is present in oxidation states (III_2,IV_2) in the native S_1 state (5, 34, 39, 40). The spectral features change significantly, along with the shift to lower energy, as the x-ray dose increases from 0.14×10^{10} to 2.3×10^{10} photons per μm^2 (4–66% of the average dose of 3.5×10^{10} photons per μm^2 used for x-ray diffraction studies), and the XANES spectrum of the PS II crystals begins to resemble that

of aqueous Mn(II) (black line) shown in Fig. 1*D*. A similar trend is observed for PS II solution samples as shown in Fig. 1*B*. The damage to the crystals is also independent of the mosaicity of the crystals. The amount of Mn(II) present in the exposed S_1 state samples is a measure of the x-ray-induced photoreduction of the Mn_4Ca complex and can be quantitated as shown in Fig. 1*C*. XANES spectra are very sensitive markers of the amount of Mn(II) and have been used in several studies to quantitate and establish the damage or contamination of native PS II with Mn(II) (41, 42).

The content of Mn(II) produced in the single crystals at 100 K as a function of the dose of 13.3-keV x-ray photons per μm^2 is shown in Fig. 2 (solid blue line). There is a rapid rise in the generation of Mn(II), followed by a slower phase. Remarkably, even at 4% of the average dose used in crystallography, 15% of Mn in the cluster is reduced to Mn(II), and the generation of Mn(II) rapidly rises, reaching a value of 80% Mn(II) at 66% of the average dose. This result shows that, even at very modest doses, much of the Mn in the PS II crystals is photoreduced to Mn(II) during the diffraction studies.

The Mn(II) generated in PS II solution samples as a function of x-ray exposure follows the same trend seen in crystals (dashed blue line, Fig. 2). The solution samples are slightly more prone to damage; however, the differences are small. We can speculate that the damage is a function of the water content, because it is known that x-ray-induced damage can be mediated by hydroxyl radicals (43). The damage and Mn(II) formation are significantly mitigated by lowering the sample temperature from 100 to 10 K during exposure (see Fig. 4, which is published as supporting information on the PNAS web site). The damage decreases by >50% for a similar dose (red line, Fig. 2), probably because of the decrease in the diffusion of the radicals generated by x-rays.

The damage to the Mn_4Ca cluster as monitored by the generation of Mn(II) is much higher at the lower energies (1.89 Å, 6.6 keV, and 100 K), where the anomalous diffraction studies are carried out (dashed green line, Fig. 2). This increase is expected because the x-ray absorption cross section of the PS II matrix, mostly composed of C, N, and O atoms, is higher at 6.6 keV compared with the cross section at 13.3 keV (see Fig. 5, which is published as supporting information on the PNAS web site). These results illustrate the extreme difficulties of collecting anomalous diffraction data. The damage is even greater at 5.5 keV (2.25 Å), where one of the anomalous diffraction data sets was collected (16) to identify electron density from Ca in the Mn_4Ca complex.

The time of exposure was not a critical parameter for Mn(II) generation at either 10 or 100 K for 13.3 or 6.6 keV x-ray energy

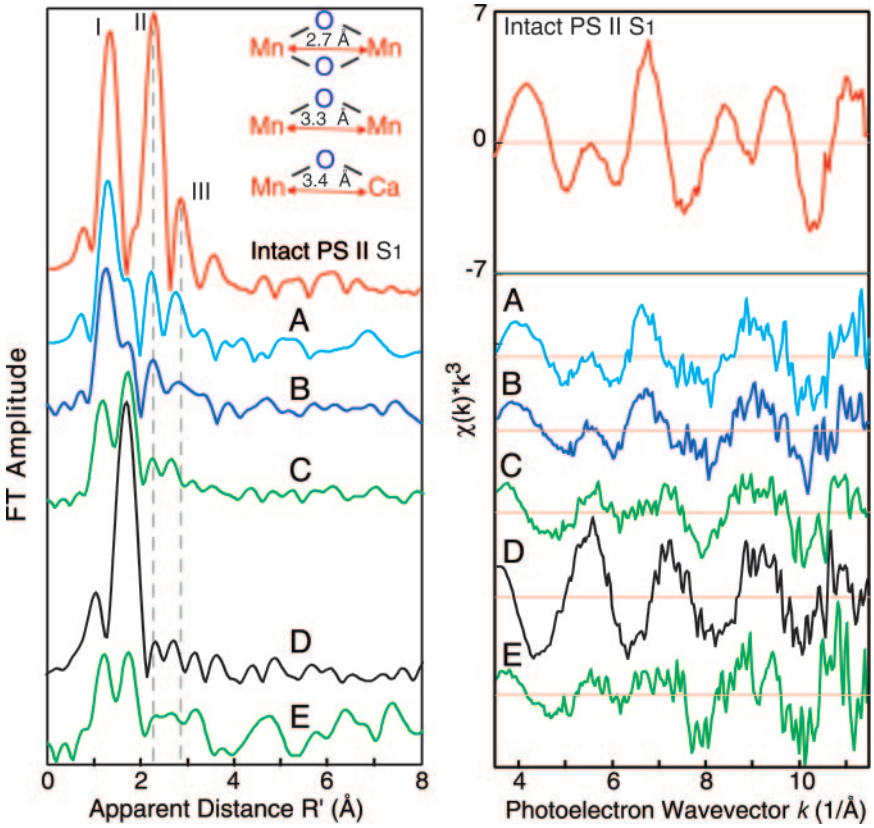

Fig. 3. Spectral changes of PS II Mn EXAFS due to radiation damage with FTs (*Left*) and the k^3-space EXAFS (*Right*). (*Left*) The FT of the EXAFS spectrum from an intact PS II solution sample is on top (red). The three Fourier peaks are characteristic of a bridged Mn_4Ca complex, with peak I from bridging Mn-oxo and Mn-terminal ligand atoms, peak II from Mn–Mn distances at 2.7 Å characteristic of di-μ-oxo-bridged moieties, and peak III from mono-μ-oxo-bridged Mn–Mn distances at 3.3 Å and Mn–Ca distances at 3.4 Å. The FTs from PS II solution samples exposed to 0.05, 0.1, 0.3, and 1.4×10^{10} photons per μm^2 at 13.3 keV and 100 K and containing 25% (blue), 35% (dark blue), 45% (green), and 90% (black) photoreduced Mn(II) are labeled A, B, C, and D, respectively. The points A, B, C, D, and E are also labeled in Fig. 2. Spectrum E (green) is from a PS II crystal exposed to 0.4×10^{10} photons per μm^2 at 13.3 keV and 100 K containing 47% Mn(II). The Fourier peaks exhibit drastic changes as the percentage of Mn(II) increases. Peak II and peak III (vertical dashed gray lines) that are characteristic of Mn–Mn distances at 2.7, 3.3, and 3.4 Å decrease and disappear along with peak I, which is due to Mn-oxo-bridging atoms. The results are similar for PS II solution and crystal samples. (*Right*) Corresponding k^3-space EXAFS spectra of PS II samples. The EXAFS modulations from the intact PS II spectrum contain several sinusoidal components, as expected from a bridged multinuclear Mn_4Ca complex. The spectrum of sample D is significantly different in both frequency and phase of the modulations, with just one sinusoidal oscillation, as one would expect from a symmetric hexacoordinated Mn(II) species with one shell of backscattering atoms. The spectra from samples A, B, and C are intermediate, with considerable damping in the amplitude and changes in the frequency components to the spectra.

exposure, because similar amounts of Mn(II) were generated after an intense exposure over a short period or a less intense exposure over a longer period (a factor of four difference in time for the same dose; data not shown). The time used to deliver the dose was varied from seconds to hours in this experiment. These results show that the total number of photons, the temperature of exposure, and the energy of x-rays are the predominant factors for the photoreduction of the Mn_4Ca cluster in PS II.

The unequivocal conclusion is that the native multinuclear Mn_4Ca complex that is present in oxidation states (III_2,IV_2) in the S_1 state of PS II is photoreduced to Mn(II) at x-ray doses typically used in the published x-ray crystallography studies.

Reduction of Mn in PS II as shown by XANES is evidence of damage to the structure of the Mn_4Ca complex (41). An even more direct measure of this damage to the structural integrity of the Mn_4Ca complex is available from Mn EXAFS studies (see *Supporting Materials and Methods* for details). In Fig. 3, the Fourier transforms (FTs) of Mn EXAFS of PS II solution samples exposed to different doses of x-rays and containing 25% (spectrum A), 35% (spectrum B), 45% (spectrum C), and 90% (spectrum D) photoreduced Mn(II) are compared with the FT from an intact PS II sample (the *k* space EXAFS spectra are shown in Fig. 3 *Right*). EXAFS from single crystals were also collected, albeit with a poorer signal-to-noise ratio, to confirm our results from PS II solutions after selected doses. Spectrum E in Fig. 3 shows the FT of the EXAFS of PS II crystals after irradiation with a dose similar to that used for spectrum C [containing 47% photoreduced Mn(II)], confirming that the observed structural changes are similar in crystals and in solution. The spectra denoted A–E correspond to the points A–E shown in Fig. 2.

The FT of the intact PS II sample (Fig. 3) is consistent with numerous spectra published over the years by our group and others (5, 39, 44–46). The Fourier peak labeled I is characteristic of two to three 1.8-Å Mn oxo-bridging and two to three 2.0-Å Mn–O/N-terminal ligand distances per Mn atom. The peak labeled II is best fit to two to three di-μ-oxo-bridged Mn–Mn interactions at $\approx$2.7 Å, and the peak labeled III is from one mono-μ-oxo-bridged Mn–Mn and two Mn–Ca interactions at 3.3 and 3.4 Å, respectively. The presence of these three Fourier peaks is diagnostic and a requisite marker for the presence of an intact bridged multinuclear $Mn_4(III_2,IV_2)Ca$ complex.

The changes in FTs (Fig. 3), reflecting structural changes and the integrity of the Mn_4Ca complex, are dramatic. In sample A (25% Mn(II) content), there is a significant decrease in the amplitude of Fourier peak I that results from Mn-oxo-bridging ligands, along with an increase in peak intensity between peak I and II, which is typical of Mn(II)-O/N ligand distances of 2.1–2.2 Å. Peak II, characteristic of Mn–Mn interactions at 2.7 Å, also significantly decreases in amplitude, along with the appearance of a new peak that fits to Mn–Mn interaction at 3.0 Å. The best fit (for details, see Table 1, which is published as supporting information on the PNAS web site) to the data are one Mn–Mn interaction at $\approx$2.8 Å and another at the distance of $\approx$3.0 Å that is not present in native samples. Peak III, characteristic of Mn–Mn at 3.3 and Mn–Ca at 3.4 Å, is now greatly reduced in amplitude (it is obscured by the new FT peak), and there is one Mn–Mn interaction at $\approx$3.3 Å with a significantly larger disorder (Debye–Waller) parameter. This analysis shows that the Mn_4Ca cluster has been seriously disrupted along with the reduction of Mn in the cluster to Mn(II). It is conceivable that only one Mn–Mn di-μ-oxo-bridging unit (compared with three present in native samples) is retained at this level of damage.

In sample D [80% Mn(II)], the three FT peaks are replaced by a single prominent Fourier peak at an apparent distance of 1.9 Å (2.1 Å from EXAFS fits; see Table 1), which is characteristic of terminal Mn–ligand distances in Mn(II) complexes. A bridged Mn_4Ca complex is absent.

The changes in the FTs and fits for samples B and C [35% and 45% Mn(II) content], are intermediate between those seen in samples A and D .

The evidence for damage to the Mn_4Ca complex by exposure to an x-ray dose typical of the x-ray crystallography experiment[¶¶] is incontrovertible, and the inescapable conclusion is compelling: The bridged Mn_4Ca complex with Mn–Mn, Mn–Ca, and Mn-oxo-bridging distances is disrupted and is replaced by Mn(II) that is similar to Mn(II) in solution. Moreover, this disruption begins to occur in a significant manner at a low x-ray dose (point A) and increases dramatically when the dose is increased (points B, C, and D). It is evident that the bridged Mn_4Ca complex is absent at dose levels comparable to those used for x-ray diffraction. Apart from limited resolution (3.2–3.8 Å), the diffuse nature and the differences in the electron density among the four studies (14–17) probably result from a heterogeneous mixture of damaged Mn_4Ca complex and aqueous Mn(II). The damage may also alter the positions of the putative Mn/Ca ligands (13, 20, 21). Hence, it is premature to either include or exclude proposed mechanisms for oxygen evolution on the basis of the current structural model from x-ray crystallography (16).

It is well recognized that radiation damage is a serious and inherent problem in x-ray crystallography, leading to a loss of resolution and an increase in mosaicity and the overall B factor (24, 43, 47, 48). Inspection of consecutive diffraction frames (see Fig. 6, which is published as supporting information on the PNAS web site) shows that such effects are significant for PS II crystals. Clearly, the effects of a high dose are not limited to decay of the diffracting power of the crystal, but highly specific changes leading to cleavage of disulfide bonds and decarboxylation of aspartic and glutamic acid residues occur at much lower dose (29, 47, 49). This mode of damage is especially true of solvent-exposed regions of proteins but also of active sites of enzymes, which, by their very nature, are accessible to water and therefore more susceptible to damage (24, 47). In proteins that contain redox-active metals, the reduction of the metal site and structural damage can be even more severe, as recognized for heme and Cu proteins two decades ago by Chance *et al.* (30, 50) and established quantitatively in this study. The Mn_4Ca cluster should by its very nature be sensitive to x-ray radiation, because it is accessible to water molecules, and the Mn and Ca ions are coordinated predominantly by the carboxylate side chains of the protein.

It should be recognized that in the presence of redox-active metals, structural damage to the metal site could precede loss of diffractivity by two orders of magnitude of x-ray dose. This study provides ways for monitoring and decreasing the x-ray damage to the Mn_4Ca complex in PS II and for other redox-active metalloproteins. It is imperative that the position of the crystal is changed often and that more crystals are used for data collection. The temperature should be decreased from 100 to 10 K, because metal reduction and concomitant structural damage are thereby significantly mitigated. Finally, increasing the energy of x-rays from 6.6 (1.894 Å) to 13.3 keV (0.933 Å) significantly decreases radiation damage to the cluster; therefore, raising the energy further to 20–25 keV (0.6–0.5 Å) (24, 51) should be explored.

We thank Profs. George Christou (University of Florida, Gainesville) and William Armstrong (Boston College, Chestnut Hill, MA) and members of their laboratories for providing the Mn complexes and

[¶¶]The electron density is derived from a combination of diffraction data from all of the frames collected at a segment of the crystal. Hence, the last frame is exposed to a larger dose than the first frame, and the degree of damage can be quantitatively obtained from the curve in Fig. 2, thus determining the average Mn(II) present during the study. For example, if the accumulated x-ray dose is 3.5×10^{10} photons per μm^2, the amount of Mn(II) at the end of the exposure is 90%, but the average amount present during the exposure is 71% (see Fig. 7, which is published as supporting information on the PNAS web site).

Dr. Edward Berry and Profs. Karl Wieghardt and Janos Hajdu for reading the manuscript and offering helpful comments. We are grateful to Profs. Horst-T. Witt and Melvin P. Klein (1921–2000) for their encouragement in initiating this project. This work was supported by National Institutes of Health (NIH) Grant GM 55302; the Director of the Office of Science, Basic Energy Sciences, Division of Chemical Sciences, Geosciences, and Biosciences of the Department of Energy (DOE) under Contract DE-AC03-76SF00098; and the Deutsche Forschungsgemeinschaft (SFB 498, TP A4, C7, and Me 1629/2-3). Synchrotron facilities were provided by Stanford Synchrotron Radiation Laboratory (SSRL) and Advanced Photon Source, operated by the DOE, Office of Basic Energy Sciences. The SSRL Biotechnology Program is supported by the NIH National Center for Research Resources Biomedical Technology Program and by the DOE Office of Biological and Environmental Research. BioCAT is a NIH-supported research center.

1. Sauer, K. (1980) *Acc. Chem. Res.* **13,** 249–256.
2. Rutherford, A. W., Zimmermann, J.-L. & Boussac, A. (1992) in *The Photosystems: Structure, Function, and Molecular Biology*, ed. Barber, J. (Elsevier, Amsterdam), pp. 179–229.
3. Debus, R. J. (1992) *Biochim. Biophys. Acta* **1102,** 269–352.
4. Ort, D. R. & Yocum, C. F. (1996) *Oxygenic Photosynthesis: The Light Reactions* (Kluwer, Dordrecht, The Netherlands).
5. Yachandra, V. K., Sauer, K. & Klein, M. P. (1996) *Chem. Rev.* **96,** 2927–2950.
6. Yachandra, V. K. (2002) *Philos. Trans. R. Soc. London B* **357,** 1347–1357.
7. Sauer, K. & Yachandra, V. K. (2004) *Biochim. Biophys. Acta* **1655,** 140–148.
8. Britt, R. D. (1996) in *Oxygenic Photosynthesis: The Light Reactions*, eds. Ort, D. R. & Yocum, C. F. (Kluwer, Dordrecht, The Netherlands), pp. 137–164.
9. Carrell, T. G., Tyryshkin, A. M. & Dismukes, G. C. (2002) *J. Biol. Inorg. Chem.* **7,** 2–22.
10. Hasegawa, K., Ono, T.-A., Inoue, Y. & Kusunoki, M. (1999) *Chem. Phys. Lett.* **300,** 9–19.
11. Brudvig, G. W. (1995) *Adv. Chem. Ser.* **246,** 249–263.
12. Chu, H.-A., Hillier, W., Law, N. A. & Babcock, G. T. (2001) *Biochim. Biophys. Acta* **1503,** 69–82.
13. Debus, R. J., Strickler, M. A., Walker, L. M. & Hillier, W. (2005) *Biochemistry* **44,** 1367–1374.
14. Zouni, A., Witt, H.-T., Kern, J., Fromme, P., Krauβ, N., Saenger, W. & Orth, P. (2001) *Nature* **409,** 739–743.
15. Kamiya, N. & Shen, J. R. (2003) *Proc. Natl. Acad. Sci. USA* **100,** 98–103.
16. Ferreira, K. N., Iverson, T. M., Maghlaoui, K., Barber, J. & Iwata, S. (2004) *Science* **303,** 1831–1838.
17. Biesiadka, J., Loll, B., Kern, J., Irrgang, K. D. & Zouni, A. (2004) *Phys. Chem. Chem. Phys.* **6,** 4733–4736.
18. Peloquin, J. M., Campbell, K. A., Randall, D. W., Evanchik, M. A., Pecoraro, V. L., Armstrong, W. H. & Britt, R. D. (2000) *J. Am. Chem. Soc.* **122,** 10926–10942.
19. Cinco, R. M., Robblee, J. H., Messinger, J., Fernandez, C., Holman, K. L. M., Sauer, K. & Yachandra, V. K. (2004) *Biochemistry* **43,** 13271–13282.
20. Chu, H. A., Hillier, W. & Debus, R. J. (2004) *Biochemistry* **43,** 3152–3166.
21. Kimura, Y., Mizusawa, N., Yamanari, T., Ishii, A. & Ono, T. (2005) *J. Biol. Chem.* **280,** 2078–2083.
22. Messinger, J. (2004) *Phys. Chem. Chem. Phys.* **6,** 4764–4771.
23. Dau, H., Liebisch, P. & Haumann, M. (2004) *Phys. Chem. Chem. Phys.* **6,** 4781–4792.
24. Garman, E. & Nave, C. (2002) *J. Synchrotron Radiat.* **9,** 327–328.
25. Henderson, R. (1990) *Philos. Trans. R. Soc. London B* **241,** 6–8.
26. Debenham, J. M., Hao, Q., Hasnain, S. S., Dodd, F. E., Abraham, Z. H. L. & Eady, R. R. (1996) *J. Synchrotron. Radiat.* **3,** 14–19.
27. Schlichting, I., Berendzen, J., Chu, K., Stock, A. M., Maves, S. A., Benson, D. E., Sweet, R. M., Ringe, D., Petsko, G. A. & Sligar, S. G. (2000) *Science* **287,** 1615–1622.
28. Berglund, G. I., Carlsson, G. H., Smith, A. T., Szöke, H., Henriksen, A. & Hajdu, J. (2002) *Nature* 463–468.
29. Garman, E. (2003) *Curr. Opin. Struct. Biol.* **13,** 545–551.
30. Chance, B., Angiolillo, P., Yang, E. K. & Powers, L. (1980) *FEBS Lett.* **112,** 178–182.
31. Carugo, O. & Carugo, K. D. (2005) *Trends Biochem. Sci.* **30,** 213–219.
32. Robblee, J. H., Messinger, J., Cinco, R. M., McFarlane, K. L., Fernandez, C., Pizarro, S. A., Sauer, K. & Yachandra, V. K. (2002) *J. Am. Chem. Soc.* **124,** 7459–7471.
33. Kern, J., Loll, B., Luneberg, C., DiFiore, D., Biesiadka, J., Irrgang, K. D. & Zouni, A. (2005) *Biochim. Biophys. Acta* **1706,** 147–157.
34. Messinger, J., Robblee, J. H., Bergmann, U., Fernandez, C., Glatzel, P., Visser, H., Cinco, R. M., McFarlane, K. L., Bellacchio, E., Pizarro, S. A., *et al.* (2001) *J. Am. Chem. Soc.* **123,** 7804–7820.
35. Wemple, M. W., Adams, D. M., Folting, K., Hendrickson, D. N. & Christou, G. (1995) *J. Am. Chem. Soc.* **117,** 7275–7276.
36. Cinco, R. M., Rompel, A., Visser, H., Aromí, G., Christou, G., Sauer, K., Klein, M. P. & Yachandra, V. K. (1999) *Inorg. Chem.* **38,** 5988–5998.
37. Chan, M. K. & Armstrong, W. H. (1991) *J. Am. Chem. Soc.* **113,** 5055–5057.
38. Chan, M. K. (1986) Ph.D. thesis (University of California, Berkeley).
39. Penner-Hahn, J. E. (1998) *Struct. Bonding (Berlin)* **90,** 1–36.
40. Glatzel, P., Bergmann, U., Yano, J., Visser, H., Robblee, J. H., Gu, W. W., de Groot, F. M. F., Christou, G., Pecoraro, V. L., Cramer, S. P. & Yachandra, V. K. (2004) *J. Am. Chem. Soc.* **126,** 9946–9959.
41. Yachandra, V. K., DeRose, V. J., Latimer, M. J., Mukerji, I., Sauer, K. & Klein, M. P. (1993) *Science* **260,** 675–679.
42. Riggs, P. J., Mei, R., Yocum, C. F. & Penner-Hahn, J. E. (1992) *J. Am. Chem. Soc.* **114,** 10650–10651.
43. O'Neill, P., Stevens, D. L. & Garman, E. F. (2002) *J. Synchrotron Radiat.* **9,** 329–332.
44. MacLachlan, D. J., Hallahan, B. J., Ruffle, S. V., Nugent, J. H. A., Evans, M. C. W., Strange, R. W. & Hasnain, S. S. (1992) *Biochem. J.* **285,** 569–576.
45. Kusunoki, M., Takano, T., Ono, T., Noguchi, T., Yamaguchi, Y., Oyanagi, H. & Inoue, Y. (1995) in *Photosynthesis: From Light to Biosphere*, ed. Mathis, P. (Kluwer, Dordrecht, The Netherlands), Vol. 2, pp. 251–254.
46. Dau, H., Iuzzolino, L. & Dittmer, J. (2001) *Biochim. Biophys. Acta* **1503,** 24–39.
47. Ravelli, R. B. & McSweeney, S. M. (2000) *Structure* **8,** 315–328.
48. Burmeister, W. P. (2000) *Acta Crystallogr. D* **56,** 328–341.
49. Weik, M., Ravelli, R. B. G., Kryger, G., McSweeney, S., Raves, M. L., Harel, M., Gros, P., Silman, I., Kroon, J. & Sussman, J. L. (2000) *Proc. Natl. Acad. Sci. USA* **97,** 623–628.
50. Chance, B., Pennie, W., Carman, M., Legallais, V. & Powers, L. (1982) *Anal. Biochem.* **124,** 248–257.
51. Arendt, U. W. (1984) *J. Appl. Crystallogr.* **17,** 118–119.